Subspace-based background subtraction applied to aeroacoustic wind tunnel testing

Christopher J. Bahr[a,*], William C. Horne[b]

[a]*Aeroacoustics Branch, NASA Langley Research Center, Hampton, VA, USA*
[b]*Experimental Aero-Physics Branch, NASA Ames Research Center, Moffett Field, CA, USA*

Abstract

A subspace-based form of background subtraction is presented and applied to aeroacoustic wind tunnel data. A variant of this method has seen use in other fields such as climatology and medical imaging. The technique is based on an eigenvalue decomposition of the background noise cross-spectral matrix. Simulated results indicate similar performance to conventional background subtraction when the subtracted spectra are weaker than the true contaminating background levels. Superior performance is observed when the subtracted spectra are stronger than the true contaminating background levels, and when background data do not match between measurements. Experimental results show limited success in recovering signal behavior for data in which conventional background subtraction fails. The results also demonstrate the subspace subtraction technique's ability to maintain a physical coherence relationship in the modified cross-spectral matrix. Deconvolution results from microphone phased array data indicate that array integration methods are largely insensitive to subtraction type, and that background subtraction with appropriate background data is an effective alternative to diagonal removal.

Nomenclature

$\mathbf{B}$	= prewhitening operator for isolated background cross-spectral matrix
b	= background pressure and electronic signals which contaminate the signal of interest
CSM	= cross-spectral matrix, general acronym
d	= background pressure and electronic signals measured separate from the signal of interest
f	= frequency
$\mathbf{G}$	= $N \times N$ cross-spectral matrix
$\widehat{\mathbf{G}}$	= transformed $N \times N$ cross-spectral matrix
$\widetilde{\mathbf{G}}$	= subspace-based estimate of an $N \times N$ cross-spectral matrix
G	= spectrum
H	= Hermitian (conjugate) transpose
$\mathbf{I}$	= identity matrix
i,j	= indices
M	= Mach number
N	= microphone count
p	= pressure
s	= signal of interest
t	= time
$\mathbf{X}$	= matrix of eigenvectors of $\mathbf{G}$
$\widehat{\mathbf{X}}$	= matrix of eigenvectors of $\widehat{\mathbf{G}}$

*Corresponding author
Email address: christopher.j.bahr@nasa.gov (Christopher J. Bahr)

$\mathbf{x}$ = eigenvector of $\mathbf{G}$
γ^2 = coherence-squared
$\mathbf{\Lambda}$ = diagonal matrix of eigenvalues of $\mathbf{G}$
$\widehat{\mathbf{\Lambda}}$ = diagonal matrix of eigenvalues of $\widehat{\mathbf{G}}$
λ = eigenvalue

1. Introduction

Background noise contamination can be a significant problem in aeroacoustic wind tunnel testing. In closed test section wind tunnels, steady turbulent flow over microphones will contaminate measurements.[1] In open test section wind tunnels, transient wind gusts may impinge on microphones and contaminate measurements.[2] In both tunnel types, facility background acoustic noise will be present in the measurements. If the acoustic signals of interest are stationary and random, techniques exist that can separate contamination by spurious transient signals.[2] However, stationary contamination from steady turbulent flow over microphones and facility acoustic sources remains.

If the microphone data are used for beamforming or deconvolution analysis, diagonal removal is a means of overcoming microphone "self-noise."[1] With diagonal removal, the covariance or cross-spectral matrix (CSM) of the array microphone signals' narrowband Fourier coefficients is computed. The diagonal of this matrix, containing the autospectral terms, is set to zero and the beamforming algorithm adjusted appropriately. This technique removes from the beamforming analysis any contamination that is uncorrelated between microphones. However, it has no mechanism for analyzing individual microphone autospectra and does not remove correlated contamination such as that due to facility acoustic sources.

Background subtraction is a technique that can remove correlated contamination. With background subtraction, a reference or tare measurement is taken without the aeroacoustic source of interest present. The autospectrum or CSM of this tare measurement is subtracted from the autospectrum or CSM of the installed aeroacoustic source.[3] If the facility acoustic sources do not change between the tare and installed measurements and the facility acoustic sources are uncorrelated with the aeroacoustic source of interest, this subtraction can significantly improve the estimate of an aeroacoustic source.[4] However, if the facility background noise decreases in level during the installed measurement, nonphysical negative powers may be computed.[2] Additionally, under such situations, the meaning of cross-spectral levels becomes ambiguous.[2,5]

Many methods have been proposed to provide more robust handling of background noise contamination. Adaptive filtering is one option that may be used if a reference measurement is available.[6] Least-squares modeling using a tare CSM is another.[7] Eigenvalue analysis, where the eigenvalues and eigenvectors of the CSM related to the desired aeroacoustic sources are separated from those related to the background contamination, has been considered in many situations.[8–11] Identification of the appropriate signal and background eigenvalues and eigenvectors may require some prior knowledge or data assumptions. Some advanced analysis methods have been proposed which combine modeling of the aeroacoustic source subspace with data-driven analysis of the background contamination subspace.[12]

The proposed method in this work follows such a path, with the objective of implementing a straightforward eigenvector identification and removal technique. It is similar to prewhitening noise identification and removal methods used with covariance matrices in fields such as climatology[13] and biomedical imaging.[14] It operates under the assumption that the signal and background subspaces are orthogonal, and requires no source modeling. Derivation and implementation of both conventional background subtraction and the new method are first provided. Analysis with simulated acoustic data superimposed on background data from a real wind tunnel test is then presented. Finally, experimental data from both closed-wall and open-jet wind tunnel tests are processed with the technique.

2. Traditional Background Subtraction

For a traditional acoustic measurement of stochastic stationary signals, a pressure measurement at a microphone can be decomposed into two components,

$$p_i(t) = p_{i,s}(t) + p_{i,b}(t). \tag{1}$$

Here, $p_{i,s}(t)$ is the acoustic signal of interest at microphone i, while $p_{i,b}(t)$ is comprised of additional acoustic and hydrodynamic background pressure fluctuations observed by the microphone, along with electronic noise contaminating the microphone measurement. Assuming that $p_{i,s}(t)$ and $p_{i,b}(t)$ are uncorrelated and stationary, the steady-state autospectrum of microphone i is expressed as

$$G_{ii}(f) = G_{ii,s}(f) + G_{ii,b}(f). \tag{2}$$

This can be generalized to the cross-spectrum between microphones j and i as

$$G_{ji}(f) = G_{ji,s}(f) + G_{ji,b}(f). \tag{3}$$

For N microphones, the CSM is thus

$$\mathbf{G}(f) = \mathbf{G}_s(f) + \mathbf{G}_b(f) \tag{4}$$

Subsequent frequency dependence is suppressed in the notation.

$\mathbf{G}_s$, the CSM of the signal of interest, is the quantity of interest in this analysis. An isolated background measurement can be conducted to acquire the background CSM $\mathbf{G}_d$. Assuming the background acoustic, hydrodynamic and electronic statistics are completely unchanged from the isolated background measurement to the source measurement, then $\mathbf{G}_d = \mathbf{G}_b$ and

$$\mathbf{G} = \mathbf{G}_s + \mathbf{G}_d \tag{5}$$

so

$$\mathbf{G}_s = \mathbf{G} - \mathbf{G}_d. \tag{6}$$

Eq. (6) is the traditional background subtraction equation. When all of the assumptions hold true, this will recover the CSM of the signal of interest. However, any changes in background statistics will lead to errors. Direct subtraction may overpredict acoustic levels or predict negative autospectral levels, depending on how the background signals change between measurements. Depending on the signal-to-noise ratio and various source relationships, any number of errors may manifest in the magnitude and phase of cross-spectral terms when the background measurement does not accurately represent background levels during the aeroacoustic source measurement. These cross-spectral changes are particularly problematic because no obvious means of identifying errors are present, as opposed to the obvious error with negative autospectral levels. Finally, direct matrix subtraction may yield an estimate of $\mathbf{G}_s$ which is not positive semidefinite, which may have detrimental implications in subsequent data analysis.

3. Subspace Identification and Subtraction

The following derivation is adapted from work in climatology[13] and biomedical imaging,[14] where the method may be applied to time-delay covariance matrices. A CSM is a covariance matrix of narrowband Fourier coefficients for a given frequency. This makes it a Hermitian, positive semidefinite matrix. The eigenvalues of a Hermitian matrix, λ_i, are real. The eigenvalues of a Hermitian, positive semidefinite matrix are greater than or equal to zero, $\lambda_i \geq 0$. The matrix of eigenvectors of a Hermitian matrix, $\mathbf{X}$, is unitary.[15] The eigenvalue decomposition of the isolated background CSM is thus

$$\mathbf{G}_d = \mathbf{X}_d \mathbf{\Lambda}_d \mathbf{X}_d^H, \tag{7}$$

with $\mathbf{\Lambda}_d$ a size $N \times N$ real diagonal matrix containing the eigenvalues $\lambda_{i,d}$. $\mathbf{X}_d$, size $N \times N$, has the property $\mathbf{X}_d^H \mathbf{X}_d = \mathbf{I} = \mathbf{X}_d \mathbf{X}_d^H$.

Using this definition, an inverse matrix $\mathbf{\Lambda}_d^{-1/2}$ can be constructed. This matrix is the square root of the inverse of $\mathbf{\Lambda}_d$. It is a real diagonal matrix, with elements $1/\sqrt{\lambda_i}$ for $\lambda_i > 0$ and zero for $\lambda_i = 0$. Truncating $\lambda_i = 0$ terms, $\mathbf{\Lambda}_d^{-1/2} \mathbf{\Lambda}_d \mathbf{\Lambda}_d^{-1/2} = \mathbf{I}$. Eq. (7) can then be manipulated (truncating $\mathbf{X}$ to remove columns associated with $\lambda_i = 0$ terms) to yield

$$\mathbf{\Lambda}_d^{-1/2} \mathbf{X}_d^H \mathbf{G}_d \mathbf{X}_d \mathbf{\Lambda}_d^{-1/2} = \mathbf{I}. \tag{8}$$

Defining $\mathbf{B}_d = \mathbf{X}_d \mathbf{\Lambda}_d^{-1/2}$ as a prewhitening operator for the background CSM simplifies Eq. (8) to

$$\mathbf{B}_d^H \mathbf{G}_d \mathbf{B}_d = \mathbf{I}. \tag{9}$$

The operator can be applied to Eq. (5) and a transformed measurement CSM defined as $\widehat{\mathbf{G}} = \mathbf{B}_d^H \mathbf{G} \mathbf{B}_d$, yielding

$$\widehat{\mathbf{G}} = \widehat{\mathbf{G}}_s + \mathbf{I}. \tag{10}$$

The relationship in Eq. (10) could be leveraged in direct subtraction to recover the signal CSM. However, this may suffer from similar problems as standard CSM background subtraction. It is desirable to find a means to construct an estimate of $\mathbf{G}_s$, labeled here as $\widetilde{\mathbf{G}}_s$, which maintains the positive semidefinite property. One way to do so is through further eigenvalue analysis.

In general, eigenvalue analysis cannot be used to directly separate the matrices in Eq. (5). However, it can be used to separate the matrices in the transformed case of Eq. (10). Specifically, properties of the identity matrix and its effect on the eigenvalues and eigenvectors of another matrix in matrix addition can be leveraged. An eigendecomposition of $\widehat{\mathbf{G}}$ can be performed as

$$\widehat{\mathbf{G}} = \widehat{\mathbf{X}} \widehat{\mathbf{\Lambda}} \widehat{\mathbf{X}}^H. \tag{11}$$

As stated previously, $\mathbf{G}$ is Hermitian and positive semidefinite. Since $\mathbf{B}_d$ is invertible, this means $\widehat{\mathbf{G}}$ is also positive semidefinite. The same holds for $\widehat{\mathbf{G}}_s$. An eigendecomposition of Eq. (10) then yields

$$\widehat{\mathbf{X}} \widehat{\mathbf{\Lambda}} \widehat{\mathbf{X}}^H = \widehat{\mathbf{X}}_s \widehat{\mathbf{\Lambda}}_s \widehat{\mathbf{X}}_s^H + \mathbf{I} = \widehat{\mathbf{X}}_s \widehat{\mathbf{\Lambda}}_s \widehat{\mathbf{X}}_s^H + \widehat{\mathbf{X}}_s \mathbf{I} \widehat{\mathbf{X}}_s^H = \widehat{\mathbf{X}}_s \left(\widehat{\mathbf{\Lambda}}_s + \mathbf{I} \right) \widehat{\mathbf{X}}_s^H, \tag{12}$$

which holds due to the nature of the identity matrix and the distributive property of matrix multiplication. What this suggests is that the eigenvectors of $\widehat{\mathbf{G}}$ are the eigenvectors of $\widehat{\mathbf{G}}_s$, such that $\widehat{\mathbf{X}} = \widehat{\mathbf{X}}_s$. Additionally, it shows that the eigenvalues of $\widehat{\mathbf{G}}$ are related to the eigenvalues of $\widehat{\mathbf{G}}_s$ by $\widehat{\lambda}_i = \widehat{\lambda}_{i,s} + 1$. Since $\widehat{\mathbf{G}}_s$ is Hermitian and positive semidefinite, this means that the eigenvalues of $\widehat{\mathbf{G}}$ must be greater than or equal to unity. Eigenvalues greater than unity correspond to eigenvalue-eigenvector pairs of the signal $\widehat{\mathbf{G}}_s$, while those equal to unity correspond to eigenvalue-eigenvector pairs of the noise. Therefore, $\widetilde{\mathbf{G}}_s$ can be constructed by performing an eigenvalue decomposition of $\widehat{\mathbf{G}}$, subtracting the identity matrix from $\widehat{\mathbf{\Lambda}}$, retaining only the subspace of resultant eigenvalues greater than zero, and reconstructing a CSM based on that subspace. The signal estimate can then be transformed back to the real signal domain by

$$\widetilde{\mathbf{G}}_s = \left(\mathbf{B}_d^{-1} \right)^H \widehat{\widetilde{\mathbf{G}}}_s \mathbf{B}_d^{-1}, \tag{13}$$

where $\mathbf{B}_d^{-1} = \mathbf{\Lambda}_d^{1/2} \mathbf{X}_d^H$. $\widetilde{\mathbf{G}}_s$ is Hermitian and positive semidefinite.

To reiterate, the proposed method uses the following procedure:

- Measure both $\mathbf{G}$ and $\mathbf{G}_d$.

- Compute $\mathbf{B}_d$ based on the eigendecomposition of $\mathbf{G}_d$. Note that experimental and numerical realities may lead to some of the eigenvalues of $\mathbf{G}_d$ being infinitesimal, zero, or slightly less than zero. This necessitates a choice in an acceptable threshold in the construction of $\mathbf{B}_d$. Eigenvalues below this threshold, either due to their magnitude or possibly being computed as slightly negative, are discarded along with their corresponding eigenvectors. An alternative is to slightly perturb $\mathbf{G}_d$ to enforce positive semidefinite behavior and retain all positive eigenvalues. Methods exist for finding the nearest positive semidefinite matrix in terms of the Frobenius norm.[16] A simple MATLAB implementation of the referenced method is used in this work.[17]
- Compute $\widehat{\mathbf{G}}$ using $\mathbf{G}$ and $\mathbf{B}_d$.
- Compute $\widehat{\mathbf{\Lambda}}$ and $\widehat{\mathbf{X}}$ from the eigendecomposition of $\widehat{\mathbf{G}}$.
- Compute $\widehat{\mathbf{\Lambda}}_s = \widehat{\mathbf{\Lambda}} - \mathbf{I}$, retaining only the positive eigenvalues. This leads to a dimension reduction of $\widehat{\mathbf{\Lambda}}_s$ from $\widehat{\mathbf{\Lambda}}$.
- Define $\widehat{\mathbf{X}}_s = \widehat{\mathbf{X}}$, while retaining only the eigenvector columns associated with the retained eigenvalues of $\widehat{\mathbf{\Lambda}}_s$.
- Compute $\widehat{\widetilde{\mathbf{G}}}_s = \widehat{\mathbf{X}}_s \widehat{\mathbf{\Lambda}}_s \widehat{\mathbf{X}}_s^H$.
- Use $\mathbf{B}_d^{-1}$ to invert the prewhitening transformation and recover a rank-reduced estimate, $\widetilde{\mathbf{G}}_s$.

4. Perturbations of Background Sources

For ideal measurements where $\mathbf{G}_d = \mathbf{G}_b$, both traditional and subspace methods of background subtraction yield the correct result. The potential failings of traditional background subtraction when $\mathbf{G}_d \neq \mathbf{G}_b$ have been discussed in Section 2. These are now considered for the alternate method. Sekihara et al.[14] address this by first assuming the signal and background subspaces are orthogonal, and then discussing an error term for when they are not. This current discussion will only address the former situation in the context of subspace subtraction. It should be noted that there is no expectation that the signal and background subspaces must be orthogonal,[12] both due to signal-background interactions, as well as situations where propagation vectors from signal and background sources to the microphone array are nearly parallel. The practical effect of non-orthogonal subspaces is considered later in this work.

Four perturbation scenarios are considered. In the first, a source that is not present in the separate background measurement $\mathbf{G}_d$ appears in the background of the aeroacoustic source measurement $\mathbf{G}$. Assuming that this source exists in a subspace orthogonal to the background measurement subspace, the result is trivial. This background source will be treated as an aeroacoustic source of interest and remain, contaminating the estimate $\widetilde{\mathbf{G}}_s$. The second and third scenarios involve background sources either growing or weakening in strength between the background and aeroacoustic measurements. Both can be addressed in a single discussion. The fourth, where a background source disappears prior to the aeroacoustic measurement, will be considered as a subset of the weakening of a background source when the source strength goes to zero.

For the four scenarios considered, a background measurement is conducted and $\mathbf{B}_d$ computed. The background field i associated with λ_i and $\mathbf{x}_i$ has a magnitude change of $\Delta\lambda_i$ between the background and aeroacoustic measurements. The aeroacoustic measurement CSM is thus expressed as

$$\mathbf{G} = \mathbf{G}_s + \mathbf{G}_d + \Delta\lambda_i \mathbf{x}_i \mathbf{x}_i^H. \tag{14}$$

Multiplying by the prewhitening operator and its conjugate transpose yields

$$\widehat{\mathbf{G}} = \widehat{\mathbf{G}}_s + \mathbf{I} + \Delta\lambda_i \mathbf{B}_d^H \mathbf{x}_i \mathbf{x}_i^H \mathbf{B}_d. \tag{15}$$

The last term of Eq. (15) can be expanded as

$$\Delta\lambda_i \mathbf{B}_d^H \mathbf{x}_i \mathbf{x}_i^H \mathbf{B}_d = \Delta\lambda_i \mathbf{\Lambda}_d^{-1/2} \mathbf{X}_d^H \mathbf{x}_i \mathbf{x}_i^H \mathbf{X}_d \mathbf{\Lambda}_d^{-1/2}. \tag{16}$$

The nature of the eigenvectors is such that the product $\mathbf{X}_d^H \mathbf{x}_i$ is a column vector with value 1 for entry i and zeros elsewhere. This means the product $\mathbf{X}_d^H \mathbf{x}_i \mathbf{x}_i^H \mathbf{X}_d$ has zeros for all entries except entry i,i where it is unity. The expression from Eq. (16) thus has zeros for all entries, except for entry i,i where it has a value of $\Delta\lambda_i/\lambda_i$. Eq. (15) thus simplifies to

$$\widehat{\mathbf{G}} = \widehat{\mathbf{G}}_s + diag\left(1, \ldots, 1 + \Delta\lambda_i/\lambda_i, \ldots, 1\right). \tag{17}$$

The consequence of Eq. (17) is that for a positive $\Delta\lambda_i$ or strengthened background field, the background eigenvalues of $\widehat{\mathbf{G}}$ will be greater than unity and retained (though attenuated) by the proposed method, when they should be rejected.[14] For a negative $\Delta\lambda_i$ or weakened background source, the background eigenvalues of $\widehat{\mathbf{G}}$ will be less than unity and rejected as desired. A source that disappears, where $\Delta\lambda_i/\lambda_i = -1$, remains absent in the final computed $\widetilde{\mathbf{G}}_s$.

The overall result is that a new source is retained by this method, just as it would be by traditional background subtraction. A strengthened background source is at least partially retained by this method, again just as it would be by traditional background subtraction. A weakened background source is properly rejected by this method, while depending on the specific source strengths, traditional background subtraction could yield negative powers. A disappearing source, where traditional background subtraction could yield negative powers, is properly handled by this method. The proposed method thus has the potential to have superior performance when compared with traditional background subtraction, at least when the assumption of orthogonal aeroacoustic and background source subspaces holds. Note that these are narrowband methods. Frequency shifts in source characteristics between background and aeroacoustic acquisitions, for example a fan RPM change in a facility with a loud drive system and noticeable narrowband tones, will still not be handled accurately by either method.

5. Validation with Simulated Signals

As a first step of validation, the method is applied to a problem with a known solution and compared in behavior to traditional background subtraction. This is best done with an analytic acoustic source for which the exact solution is precisely known. This single-source solution will yield a signal CSM with one nonzero eigenvalue. To stress both the traditional and eigenvalue-based methods, a real background acoustic measurement from a wind tunnel test is used, as opposed to simulated background sources.

The background noise data are taken from the recent Hybrid Wing Body N2A-EXTE aeroacoustic test in the NASA Langley 14- by 22-Foot Subsonic Tunnel.[18] A photograph of the test with the model installed in the facility is shown in Fig. 1. This shows the position of the array relative to the facility test section for a typical model configuration, as well as labels for aerodynamic sources of interest discussed later in this work. For the considered cases, empty tunnel data are used with the phased array center stationed 197 inches downstream from the test section inlet. Empty tunnel data for Mach numbers of $M = 0.11$, 0.17, and 0.23 are used. Array microphones showing signs of problems such as an unreliable sensitivity or faulty connection are removed from the CSM prior to processing so as not to affect the eigenvalue analysis, leaving 89 of the original 97 microphones. Note that all CSM data from the experiments are stored as single precision. These are recast to double precision for the intermediate calculations and matrix inversions to minimize potential issues with small eigenvalues (though no issues were observed with single precision calculations). While only 1 decade of the data is shown, the process is conducted on all 4096 bins of the CSMs. Run times are significantly longer than conventional background subtraction, but still only approximately 25 seconds per case with $89 \times 89 \times 4096$ CSM data arrays using a MATLAB 2015a implementation on a Macbook Pro with 16 GB of RAM and an Intel Core i7 4960HQ processor.

For ease of study, a plane wave propagating in quiescent free space is selected as the acoustic source of interest, and simulated for the phased array layout used in the test.[19] Atmospheric attenuation and microphone directivity effects are not modeled. The wave is simulated as propagating normal to the flow direction and parallel to the array face at the speed of sound computed for the $M = 0.17$ background data, and added to the $M = 0.17$ background data. The plane wave is defined to have a level of 40 dB using the preselected 30.5 Hz binwidths of the default data analysis from the test over a frequency range of 4 kHz

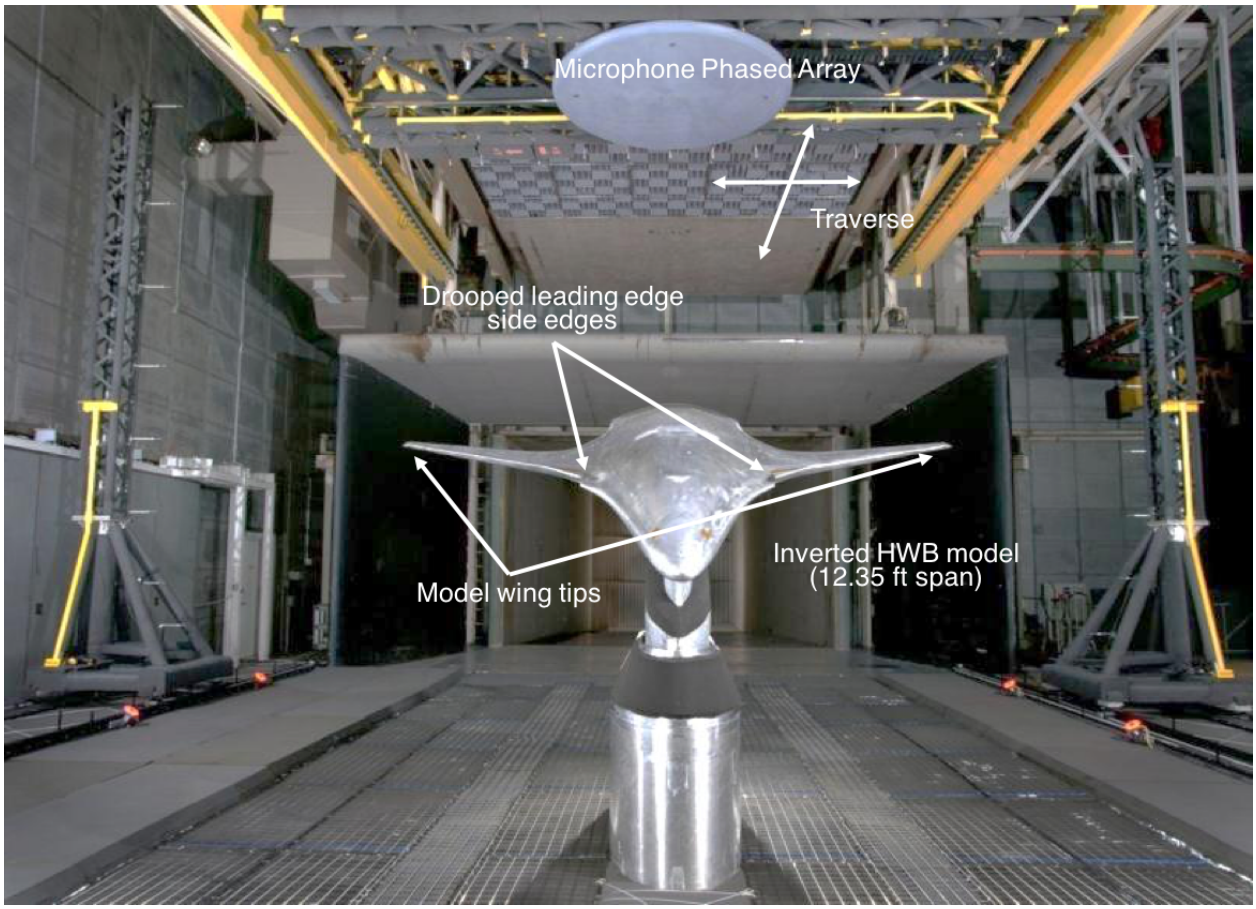

Figure 1. Example arrangement of the HWB model and phased array. Aerodynamic sources of interest on the model are labeled.

to 16 kHz, and no power at other frequencies. This gives an acoustic signal level slightly more than 11 dB below the facility background level observed by the array center microphone at 4 kHz, and slightly more than 4 dB above the background for the same microphone at 16 kHz. Discussion is limited to the 2 kHz to 20 kHz decade. Five different cases are initially considered:

1. The acoustic source summed with the $M = 0.17$ background data are processed with the $M = 0.17$ background data. Traditional background subtraction will, within floating point accuracy, identically recover the acoustic signal for this situation.
2. The acoustic source summed with the $M = 0.17$ background data are processed with the $M = 0.17$ background data, but $\mathbf{G}_d$ is artificially decreased by 3 dB prior to analysis. This simulates a gain in background levels from the background acquisition to the acoustic source acquisition. Traditional background subtraction will overpredict acoustic signal levels.
3. The acoustic source summed with the $M = 0.17$ background data are processed with the $M = 0.17$ background data, but $\mathbf{G}_d$ is artificially increased by 3 dB prior to analysis. This simulates a reduction in background levels from the background acquisition to the acoustic source acquisition. Traditional background subtraction will either underpredict acoustic signal levels or yield negative powers.
4. The acoustic source summed with the $M = 0.17$ background data are processed using the $M = 0.11$ background data. This simulates a poor estimate of the background data that is lower in level than the true background.

5. The acoustic source summed with the $M = 0.17$ background data are processed using the $M = 0.23$ background data. This simulates a poor estimate of the background data that is higher in level than the true background.

Of these five cases, only cases 2, 3 and 5 are discussed further. Case 1 is trivial and as expected, all analyses show identical correct results when comparing methods. Cases 2 and 4 show near-perfect agreement between conventional and subspace subtraction and similar behavior between the cases. As such, of the two only Case 2 is shown. The input and Case 2 results are shown in Fig. 2, while the Case 3 and Case 5 results are shown in Fig. 3. Each set of data shows the autospectral results of Microphone 1 (located at the array center), along with the cross-spectral magnitude and phase between Microphones 1 and 10. Microphone 10 is located 0.46 inches upstream and 1.14 inches laterally from the array center. The objective of all of the subtraction comparisons is to match the input source of interest spectrum.

The Case 2 autospectral results, shown in Fig. 2b, do not accurately reconstruct the signal of interest autospectrum from Fig. 2a at lower, high-background frequencies. Instead, they still trend with the source contaminated with noise. The Case 3 autospectral results, shown in Fig. 3a, show that, as expected, conventional background subtraction fails to recover the correct solution when the background acquisition is louder than the acoustic source acquisition. For sufficiently high noise values it predicts negative powers, which are zeroed in plots. At higher frequencies it simply underpredicts the acoustic signal of interest. The subspace subtraction, on the other hand, accurately recovers the signal of interest at all frequencies. Case 5, shown in Fig. 3b, behaves similarly to Case 3, with conventional subtraction failing for the full analysis bandwidth. Subspace subtraction correctly recovers the acoustic signal of interest for the bandwidth of the acoustic signal. Outside of that frequency band, some background signal is still retained. The overall picture of autospectral behavior is that the subspace method never performs worse than conventional background subtraction, and performs better in some situations where conventional subtraction fails.

The Case 2 cross-spectral magnitude results, shown in Fig. 2d, show similar behavior to the autospectral results. Neither method accurately reconstructs the cross-spectral magnitude of the signal of interest, shown in Fig. 2c, at lower frequencies. Both methods do show reasonable phase recovery in Fig. 2f when comparing to the input in Fig. 2e, for frequencies where the signal cross-spectral magnitude is the same or greater than the background cross-spectral magnitude. As with the autospectra, the Case 3 (Fig. 3c) and Case 5 (Fig. 3d) cross-spectral magnitude results demonstrate that the subspace subtraction technique recovers the signal for its full bandwidth, though it retains some background contamination outside of that band with Case 5. Conventional subtraction only recovers the cross-spectral magnitude at higher frequencies. A similar behavior is seen with the phases for Case 3 (Fig. 3e) and Case 5 (Fig. 3f). Conventional subtraction appears to have a similar cut-on for effectiveness for phase recovery when comparing Cases 2 and 3. It experiences more difficulty with Case 5. The overall picture of cross-spectral behavior is the same as that for autospectral behavior. Subspace subtraction often performs better, and never worse, than conventional subtraction.

6. Experimental Data: Auto- and Cross-Spectra

The performance evaluation of background subtraction continues with the use of experimental data. Individual auto- and cross-spectra are first considered, prior to the analysis of more complex array processing techniques. The data analyzed here come from a test campaign in the Arnold Engineering Development Center 40- by 80-Foot Wind Tunnel at the NASA Ames Research Center,[20,21] as well as the airframe noise portion of the aforementioned test in the NASA Langley Research Center 14- by 22-Foot Subsonic Tunnel.[22] While cross-spectral phase was shown in the simulated signal analysis, it is neglected subsequently. Due to the more complicated nature of the signals, plots of phase are found to differ between methods but do not contribute additional insight into the comparison of the subtraction techniques.

6.1. Inflow array

The first test considered is that using an inflow array in the 40- by 80-Foot Wind Tunnel, shown installed in the test section with the AMELIA CESTOL model in Fig. 4a. Data were acquired for an inflow speaker

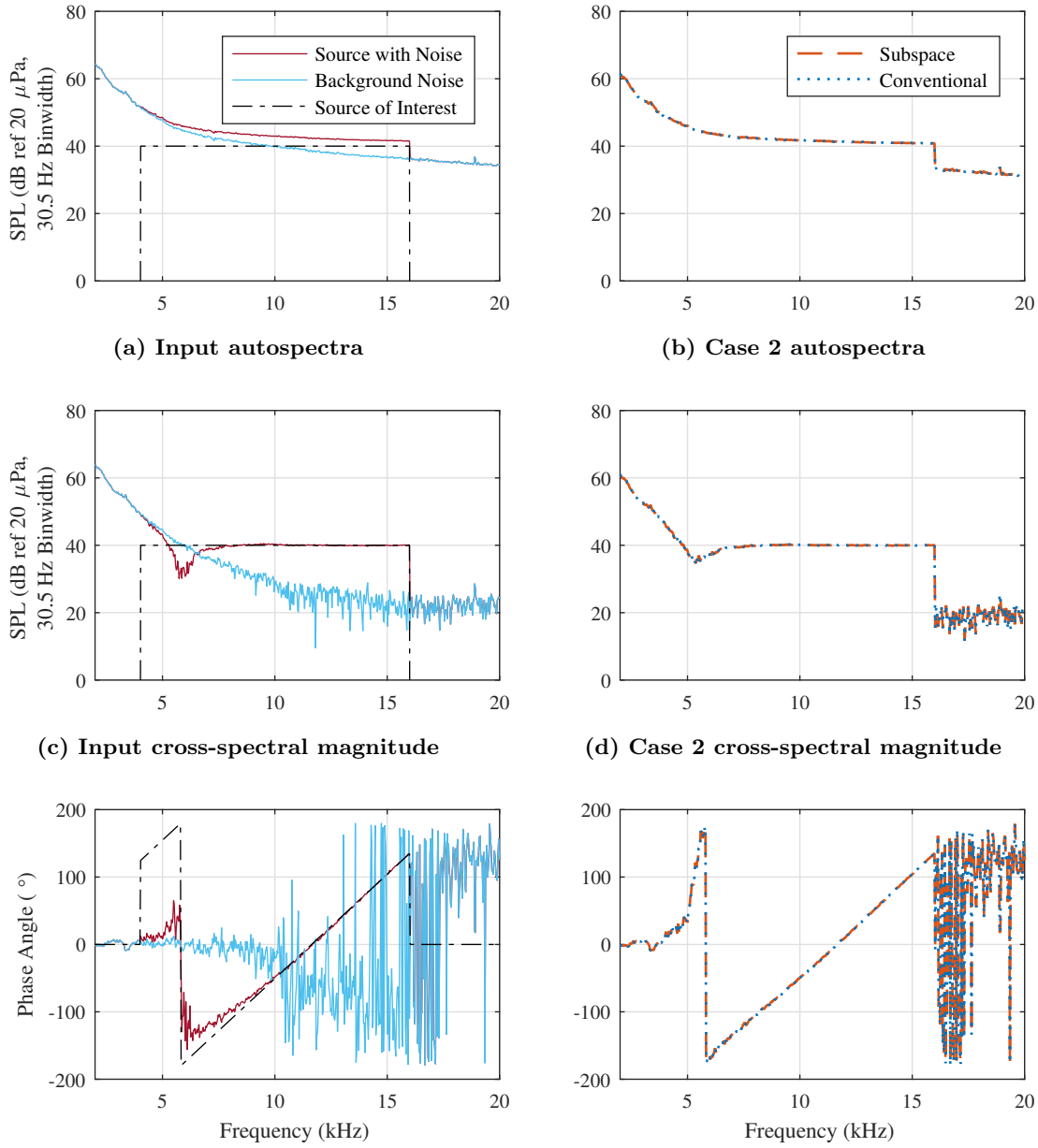

(a) Input autospectra **(b) Case 2 autospectra**

(c) Input cross-spectral magnitude **(d) Case 2 cross-spectral magnitude**

(e) Input cross-spectral phase **(f) Case 2 cross-spectral phase**

Figure 2. Inputs and Case 2 (G_d reduced by 3 dB) outputs for simulated data study. The autospectra are from microphone 1 and the cross-spectral quantities are between microphones 1 and 10.

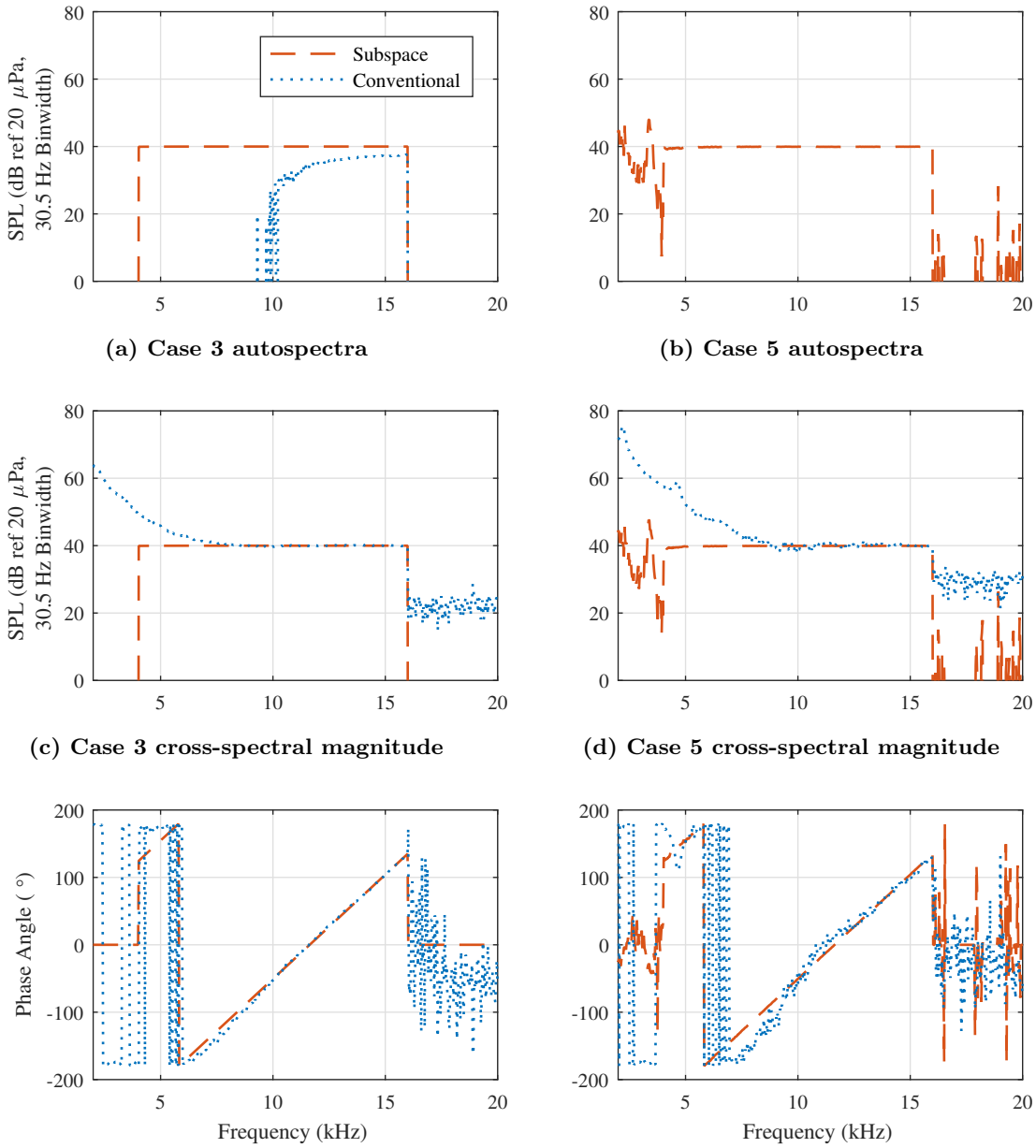

(a) Case 3 autospectra

(b) Case 5 autospectra

(c) Case 3 cross-spectral magnitude

(d) Case 5 cross-spectral magnitude

(e) Case 3 cross-spectral phase

(f) Case 5 cross-spectral phase

Figure 3. Case 3 (G_d increased by 3 dB) and Case 5 (Mach 0.23 isolated background) outputs for simulated data study. The autospectra are from microphone 1 and the cross-spectral quantities are between microphones 1 and 10.

system associated with the AMELIA CESTOL test, shown mounted to the tunnel floor in Fig. 4b. Acoustic data were recorded using an OptiNav Array 48 pattern and an in-house data acquisition system. CSMs were generated using the OptiNav Beamform Interactive software package, although the background subtraction used here is performed outside of the OptiNav tool chain. For the data considered, the facility was operated at a test section Mach number of $M = 0.2$. The inflow speaker system was installed in the test section and given a pink noise input signal at varying input voltage levels. The microphones in this setup experience some degree of self-noise from being exposed to the flow, so much of the background noise CSM consists of hydrodynamic self-noise. Greater contamination is expected in autospectra than in cross-spectra.

(a) 11% AMELIA CESTOL sting mounted model in wind tunnel; strut mounted array in lower left of image

(b) Inflow speaker fairing in place of the model

Figure 4. Overall measurement setup in the 40- by 80-Foot Wind Tunnel.

Baseline autospectra from array microphone 1 are plotted in Fig. 5a for speaker input levels of 2.8 V and 9.0 V, as well as the background level for 0.0 V. The 2.8 V signal is treated as the signal of interest here as it has a low signal-to-noise ratio for much of the considered bandwidth and warrants application of background subtraction. The 9.0 V signal is plotted as reference for the expected shape of the speaker spectrum with flow. The 2.8 V signal without flow is shown as a reference for the overall signal bandwidth and level, although flow-related influence on facility reverberance, propagation, and speaker radiation make this comparison qualitative. The 2.8 V signal (with flow) becomes nearly indiscernible from the background signal near 14 kHz, while features of the 9.0 V signal are observable up to 18 kHz. The cross-spectra between microphones 1 and 2 of the array (adjacent microphones in the pattern) for the same conditions are plotted in Fig. 5b. The cross-spectrum for the 2.8 V signal is clearly distinct from the background noise up to near 16 kHz, while it is distinct for the entire plotted bandwidth of the 9.0 V signal.

Results of background subtraction are shown in Figs. 5c and 5d. For both auto- and cross-spectra, the conventional and subspace-based subtraction methods are in agreement for frequency bands where the signal is clearly discernible from the noise. Conventional subtraction appears unreliable above approximately 14 kHz in the autospectrum. Subspace-based subtraction appears to perform somewhat better, trending in shape with the 9.0 V data though barely showing the spectral hump between 15 kHz and 18 kHz. It fully trends as an offset version of the facility background noise by 20 kHz. The subspace-based subtraction shows a smoother, more consistent behavior in bands where the background noise is dominant. For the cross-spectra, both methods trend near-perfectly with the unmodified data until approximately 16 kHz, where the background cross-spectral magnitude becomes significant relative to the signal. Neither one recovers a spectral shape similar to the 9.0 V cross-spectrum at higher frequencies.

Signal-to-noise ratio estimates are plotted in Fig. 5e, in an attempt to assess an effective noise floor of the subtraction methods for this data set. These are calculated by dividing the (autospectrum) results of background subtraction for microphone 1 by the 0.0 V background data. By its nature, this plot can only show the background-subtracted results and thus, does not have baseline 2.8 V and 9.0 V curves. Note that frequency bins with negative autospectral levels for the microphone are not plotted for conventional background subtraction. Estimates are similar below 14 kHz. They begin to significantly diverge above 14 kHz, where both methods drop below ratios of 0.5. At the higher frequencies, the subspace method tends to stay bounded between ratios of 0.1 to 0.3, while the conventional subtraction is bounded on the upper end by 0.3 and undefined on the lower end with negative estimates. The 0.1 to 0.3 range appears to bound the band where background subtraction can no longer reliably extract information about the signal of interest for the autospectrum.

Coherence-squared (γ^2) estimates between microphones 1 and 2 are plotted in Fig. 5f. These are shown for the auto- and cross-spectra computed with both subtraction methods as well as those for the baseline 2.8 V and 9.0 V signals. Note that frequency bins with negative autospectral levels for either microphone 1 or microphone 2 are not plotted for conventional subtraction. This plot emphasizes one of the main benefits of the subspace subtraction method over conventional background subtraction. Conventional subtraction, as discussed previously, is not constrained to yield a positive semidefinite estimate of $\mathbf{G}_s$. One consequence of this is that the Cauchy-Schwarz inequality is no longer guaranteed to be met by the subtracted data. For this data set at higher frequencies, conventional subtraction yields γ^2 estimates of greater than 100. Conversely, subspace-based subtraction yields a well-bounded estimate of $\gamma^2 \leq 1$. Additionally, the subspace-based subtraction yields an estimate of γ^2, which trends with the stronger, 9.0 V signal as opposed to the 2.8 V signal. While this may not have much meaning above 18 kHz where the 9.0 V signal is also dominated by background noise in its autospectra, it does lend some confidence to the overall trend of the method between 15 kHz and 18 kHz, even if individual frequency bins tend to vary noticeably from the 9.0 V data.

6.2. Out-of-flow array

The 14- by 22-Foot Subsonic Tunnel Hybrid Wing Body N2A-EXTE test used for the simulated signal analysis is now revisited, but with the model installed in the facility. During the airframe noise component of the test, one of the configurations considered involved the installation of a drooped leading edge on the model. This drooped leading edge generated noise from its exposed side edge. The following analysis assesses the ability of background subtraction to isolate drooped leading edge noise from other noise sources by subtracting the stowed leading edge configuration. This will stress both subtraction techniques, as the change in flow around the model from deploying the drooped leading edges should influence other aerodynamic noise sources such as the wing tip vortices. This leads to a change in background sources between background and source-of-interest acquisitions. Unlike the inflow array test, much of the background CSM for this test is acoustic in nature. Contamination may be equally present in both auto- and cross-spectra.

Fig. 6a shows the autospectra of the array center microphone for the drooped and stowed leading edge configurations. For both of these measurements, all other airframe components are held constant, the model is installed at a 13.1° angle of attack, and the test section Mach number is 0.17. The signal from the drooped leading edge is clearly separable from the stowed leading edge configuration above approximately 8 kHz. In the cross-spectral magnitudes of Fig. 6b, the drooped leading edge signal appears separable above 7 kHz, although it drops below the background at high frequencies due to the nature of phasor addition for complex covariances.

Background subtraction is applied and plotted in Figs. 6c and 6d. The autospectra from both background subtraction methods are in substantial agreement between 10 kHz and 15 kHz. Between 8 kHz and 10 kHz and above 15 kHz, conventional subtraction yields results of slightly lower level than the subspace-based subtraction. Below 8 kHz, the two results show significant difference in the autospectra. The cross-spectra show closer agreement down to 5 kHz, although the conventional method shows more variation in cross-spectral magnitude below 7.5 kHz.

Signal-to-noise ratio, computed by treating the stowed leading edge configuration as the noise estimate, is plotted in Fig. 6e and shows significant divergence between methods below approximately 8 kHz. Coherence-squared, plotted in Fig. 6f, shows divergence between methods below approximately 11 kHz. For conventional

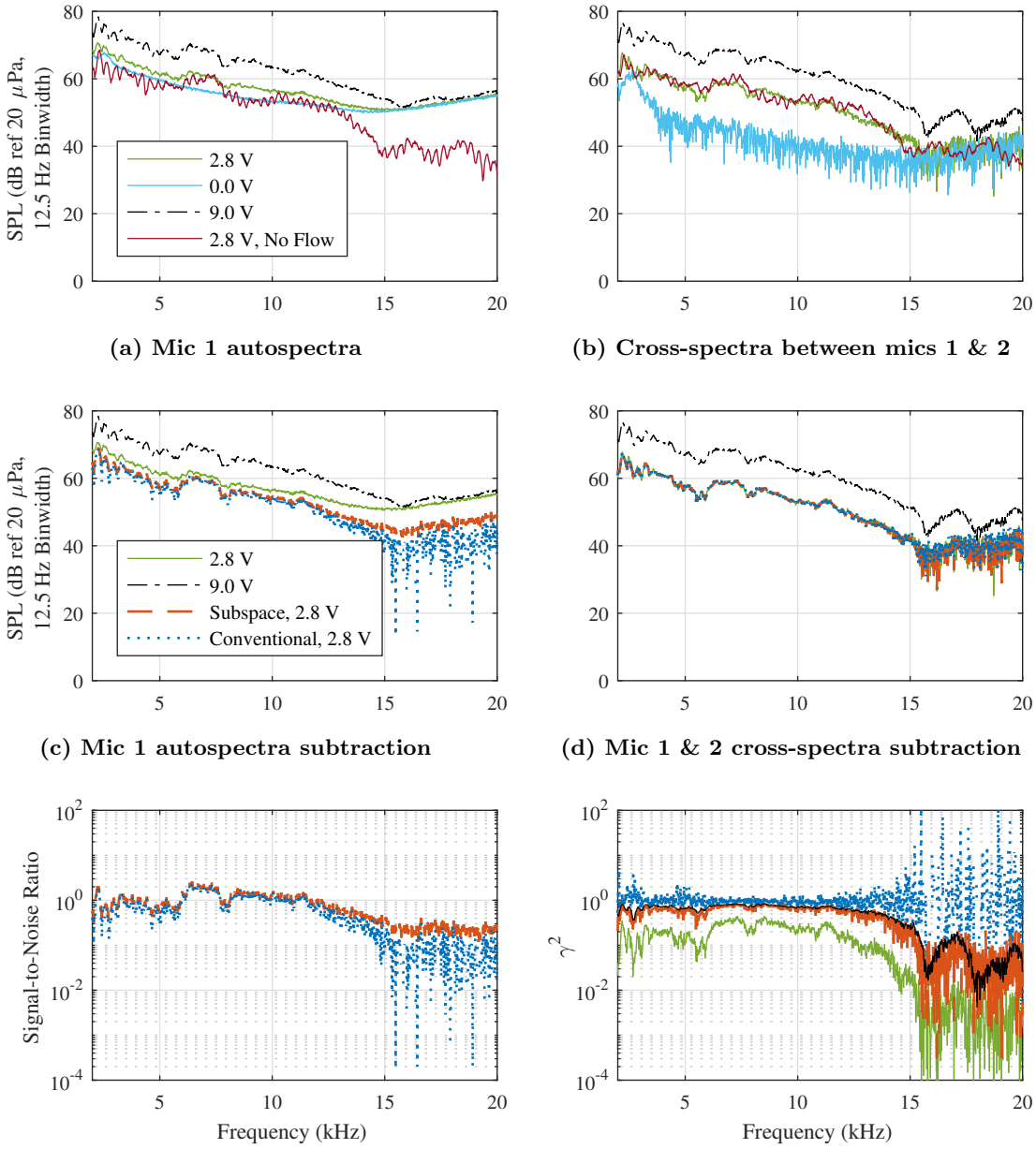

(a) Mic 1 autospectra

(b) Cross-spectra between mics 1 & 2

(c) Mic 1 autospectra subtraction

(d) Mic 1 & 2 cross-spectra subtraction

(e) Mic 1 signal-to-noise ratio

(f) Coherence-squared between mics 1 & 2

Figure 5. 40- by 80-Foot Wind Tunnel inflow Array 48 data from inflow speaker operation in otherwise empty test section, Mach 0.2.

subtraction, both values break down in this frequency band as signal-to-noise varies significantly with frequency and coherence-squared values, below 9 kHz, are greater than unity. The subspace-based subtraction appears to yield well-behaved results down to 2 kHz, although auto- and cross-spectral shapes suggest the results may be attenuated acoustic sources from the subtracted acquisition rather than the source of interest. This is assessed further through deconvolution analysis.

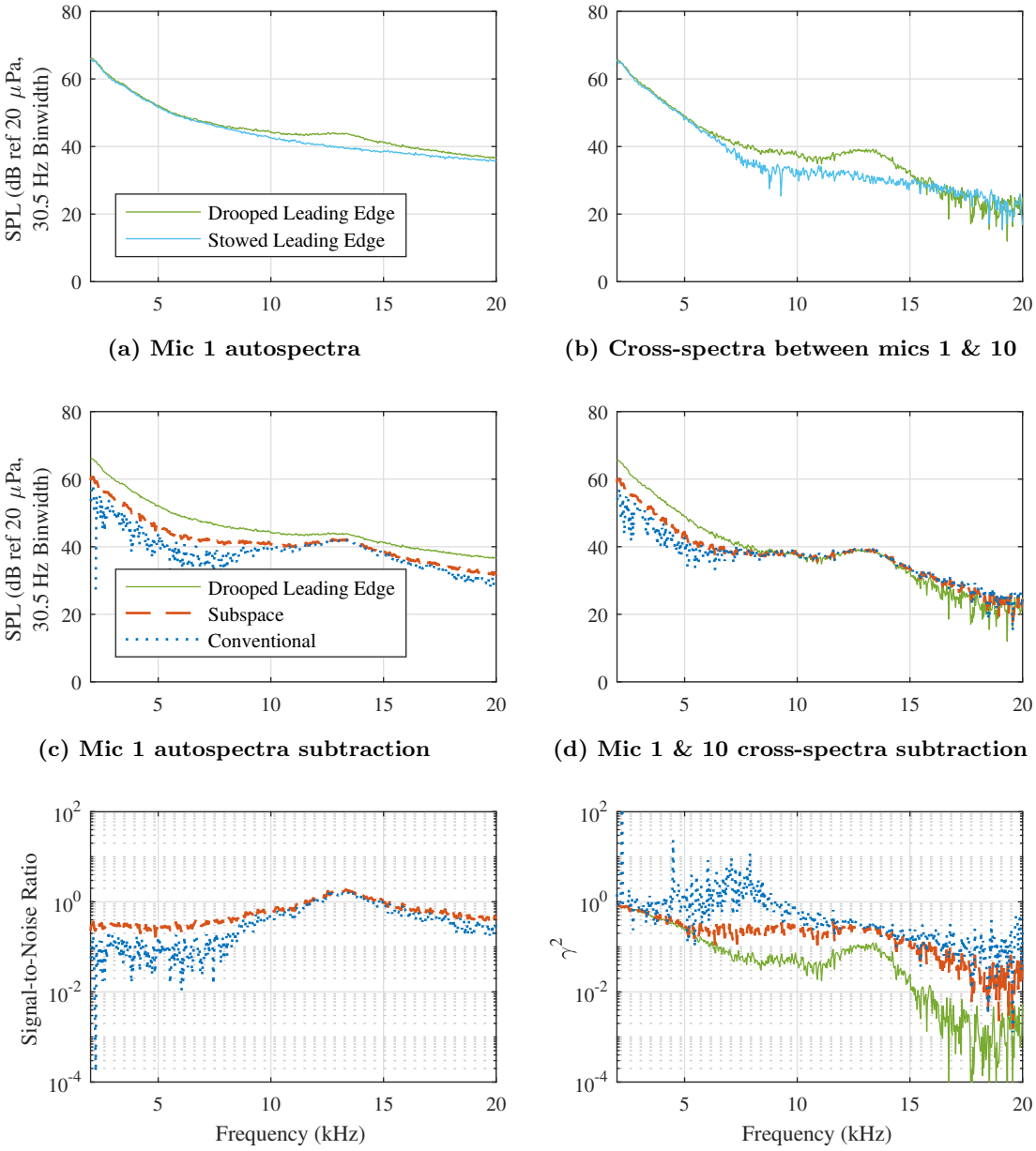

(a) Mic 1 autospectra

(b) Cross-spectra between mics 1 & 10

(c) Mic 1 autospectra subtraction

(d) Mic 1 & 10 cross-spectra subtraction

(e) Mic 1 signal-to-noise ratio

(f) Coherence-squared between mics 1 & 10

Figure 6. 14- by 22-Foot Subsonic Wind Tunnel out-of-flow phased array data for leading-edge droop with model angle of attack of 13.1° and test section Mach number of 0.17.

7. Experimental Data: Deconvolution

The two tests considered in the previous section are revisited. Analysis proceeds to the variability in phased array deconvolution results due to the background subtraction process. The influence of diagonal removal (DR) on the results is also presented.

7.1. Inflow array

The inflow array data from the 40- by 80-Foot Wind Tunnel are processed using the OptiNav software and the DAMAS2 algorithm.[23] The deconvolution map is sized to encompass the speaker installation, but not any additional facility noise sources. This prevents the discrimination of beamforming sidelobes generated by upstream and downstream facility noise propagation. The consequence of this choice is that if background subtraction is not applied, additional facility noise sources can contaminate the beamforming and deconvolution results. Diagonal removal may also be necessary to mitigate uncorrelated pressure fluctuations on the in-flow microphones, depending on the efficacy of the background subtraction. Diagonal removal serves another purpose here. If conventional subtraction yields significant negative autospectral levels, these levels may have unforeseeable effects on the deconvolution process. Diagonal removal counters this issue. For this particular discussion, integrated power levels are computed as the sum of the entire deconvolution map. For an uncontaminated single source measurement, this would yield the correct acoustic level.

Results of the deconvolution process are shown in Fig. 7. Here the data are analyzed both with and without diagonal removal and with no subtraction, conventional subtraction, and subspace subtraction. The frequency axis of the spectral plot has been changed to a logarithmic scale, in contrast to previous spectral plots, to emphasize certain differences in the spectra. For much of the plotted bandwidth, the various parameter combinations have little influence on the integration output. This could mean that a) there is minimal noise contamination in this band, b) the filtering nature of the initial beamforming step of deconvolution has already sufficiently mitigated data contamination, or c) the behavior of any data contamination is such that its influence on the deconvolution process is insensitive to the parameters that are varied. Based on the plotted single-microphone autospectrum, which features higher levels than any deconvolution results throughout the spectrum, some combination of b) and c) is most likely.

Two segments of the plotted bandwidth do show some disagreement between the spectra. The first, in the vicinity of 2.5 kHz, shows different behavior when no subtraction technique is used as compared to conventional or subspace subtraction. Diagonal removal appears to have little influence here. This is indicative of correlated noise contamination in the data CSM, likely due to an acoustic background source. The DAMAS2 deconvolution maps (computed from the 12.5 Hz narrowband CSM) are plotted in Fig. 8 for further evaluation. These source maps overlay sound pressure level on a rendering of the speaker fairing. The speakers are indicated by the black circles, and the rightmost speaker is active for this test.

As there are two groupings of spectra at 2.5 kHz, for brevity only two deconvolution maps are plotted. Within the no subtraction/subtraction groupings the maps appear similar. For all of these results, the peak level of the deconvolution output is offset from the speaker center. This is likely due to the severe look angle of the array toward the speaker due to the testing constraints in combination with the shift-invariance assumption of DAMAS2.[23] The analysis with no diagonal removal and no subtraction, shown in Fig. 8a, shows a significant secondary source region below the speaker fairing. This source could be related to aerodynamic noise generated by the fairing mount visible in Fig. 4b. Subspace subtraction, shown without diagonal removal in Fig. 8b, successfully mitigates this secondary source. This is to be expected as the background data are simply the same measurement with the speaker turned off. Ideally any form of subtraction should identically remove the fairing mount aerodynamic noise.

The second band where the spectra of Fig. 7 disagree is for frequencies above approximately 15 kHz. Here, all of the spectra begin to show more variation and spread. Two characteristic deconvolution results at 18 kHz are shown in Fig. 9. At this frequency the results with no diagonal removal and no subtraction are significantly different from the other methods, so they are shown in Fig. 9a. The map shows the same source location as the 2.5 kHz results, but with a region of substantial secondary source distribution to the left. All of the contamination treatment options show similar behavior in their deconvolution maps, so as an example the no diagonal removal, subspace subtraction map is plotted in Fig. 9b. Subtraction

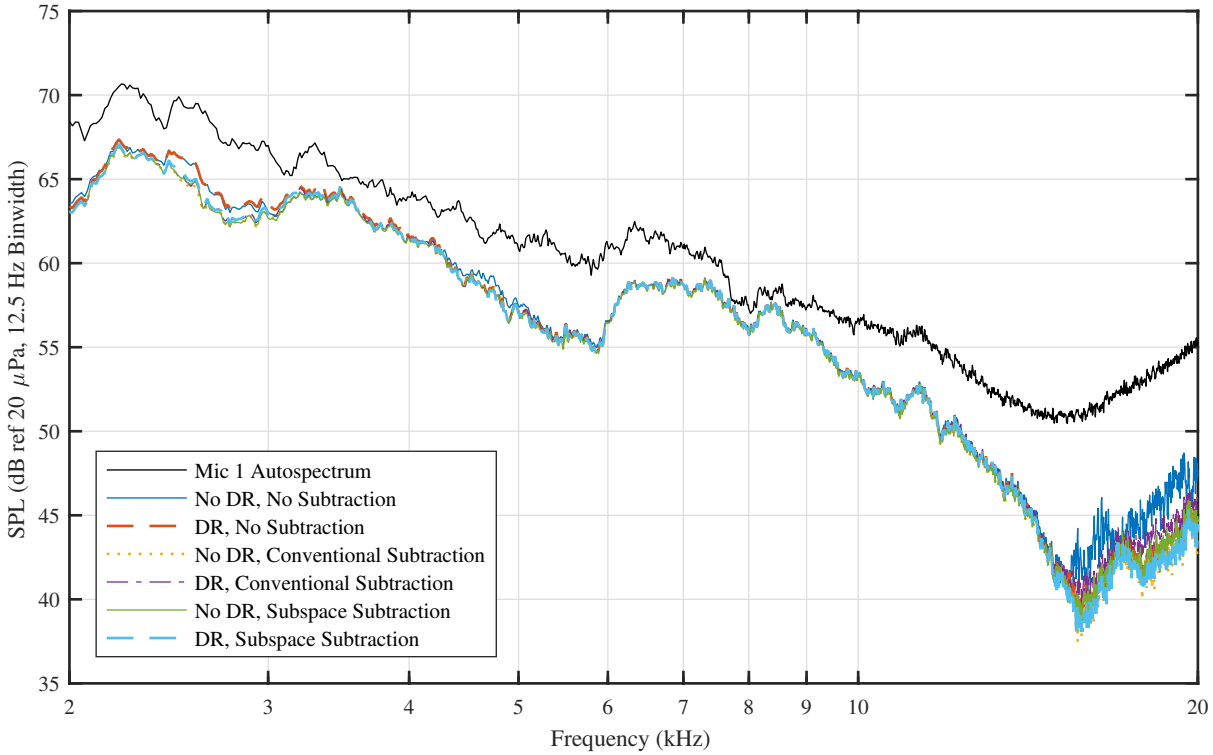

Figure 7. Comparison of DAMAS2 integrated spectra results for 40- by 80-Foot Wind Tunnel data.

mitigates the region of secondary sources, but come with the expense of significant speckle throughout the deconvolution map when a 12-dB plot range is maintained relative to the map peak. The common behavior of these various combinations of subtraction methods and diagonal removal would suggest two things. First, background subtraction and diagonal removal have the same effect on the results: removing uncorrelated noise contamination along the CSM diagonal. This is in agreement with the isolated spectral results of the previous section. Second, the resultant CSM still has significant contamination of some sort, possibly suggesting a change in the background sources from background to source acquisition. Alternatively, an effect such as turbulent decorrelation could be influencing the off-diagonal terms of the CSM and degrading the results of all the analysis methods.[24]

7.2. Out-of-flow array

The out-of-flow array data from the 14- by 22-Foot Wind Tunnel are processed using in-house software and the DAMAS algorithm.[25] Details of the selected processing parameters can be found in the initial study of this method.[26] As with the inflow array data, the deconvolution map is sized to encompass the source of interest, here the entire aircraft model, but not include regions from which facility noise sources may propagate. This means that, ideally, deconvolution should be able to successfully separate noise sources from the airframe depending on integration bounds, but will still fail to properly mitigate contamination from sources outside of the deconvolution map region.

As discussed with the individual auto- and cross-spectra for these data, it is expected that there will be a change in background noise source behavior between the selected background and source-of-interest acquisitions. The aerodynamic dependency of the wing tip vortices on the deployment of the drooped leading edges may lead to a violation of the source independence assumption. Additionally, in general, propagation vectors from geometrically-close sources to a somewhat distant microphone array may be nearly parallel, grossly violating the orthogonality assumption in this analysis. Therefore, one additional subtraction technique, which

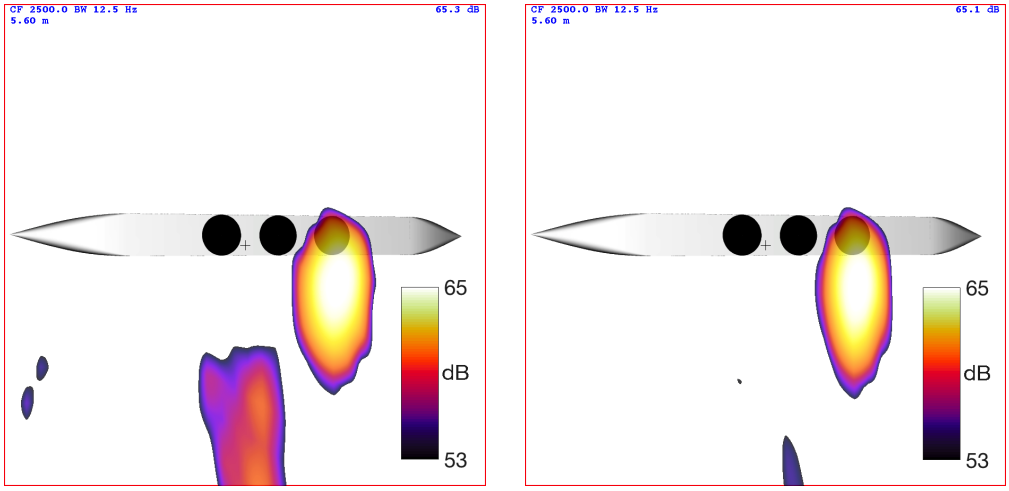

(a) No DR, no subtraction **(b) No DR, subspace subtraction**

Figure 8. Comparison of DAMAS2 2.5 kHz narrowband deconvolution results for 40- by 80-Foot Wind Tunnel data. Images have a 12-dB dynamic range.

allows for a non-orthogonal, or oblique, relationship between background and source-of-interest subspaces, is applied to the data.[12] Oblique subtraction involves estimating the angle between the source-of-interest and background subspaces. This angle is then used to project the measurement data onto the source-of-interest subspace. The technique, while more computationally-intensive for large analysis grids, may prove more robust with generalized background-source relationships. Note that in the reference, the final step of the oblique subtraction analysis applies a covariance matrix-fitting procedure rather than a DAMAS-like deconvolution analysis.[27] While using the fitting approach may be necessary for the best performance of the oblique projection process, this current analysis simply applies DAMAS to the resultant CSM so algorithm selection does not influence any variability in the results. For this case, integrated levels are computed by summing the power contained in 20" by 20" squares drawn around the inboard side edges of the drooped leading edges and the airframe wing tips. Integration bounds are superimposed on all deconvolution maps.

Results of the deconvolution process for the drooped leading edge side edges are shown in Fig. 10. The data are analyzed both with and without diagonal removal and with no subtraction, conventional subtraction, orthogonal subspace subtraction, and oblique subspace subtraction. The frequency axis of the spectral plot has been returned to a linear scale for easiest viewing of the data. As with the inflow array data, for much of the plotted bandwidth, the various parameter combinations have little influence on the integration output. The reasons suspected for the similarity in the method outputs are the same as those for the inflow data. Since diagonal removal and subtraction both have similar effects on the integrated spectra, this suggests that much of what any subtraction technique is removing from the drooped leading edge side edge signal lies along the CSM diagonal and is uncorrelated between microphones, in agreement with the isolated spectral results of the previous section above 8 kHz. Below 8 kHz, this would suggest that while the cross-spectra may experience some change during subtraction, the autospectra play a more dominant role in the deconvolution output.

For reference, the integrated wing tip spectra are calculated for every condition and compared to the total wing tip spectrum from the stowed leading edge measurement in Fig. 11. Were the subtraction ideal, the background data would perfectly overlay the drooped leading edge processing without subtraction, and all subtraction methods would yield zero power. Instead the figure shows approximately 5-6 dB reduction at high frequencies for all subtraction methods, even less reduction at low frequencies (neglecting the low frequency background diagonal removal case), and maximum rejection in the mid-frequency band from 6 kHz to 12 kHz. Much of this frequency range is where the wing tip sources appear to reduce in magnitude

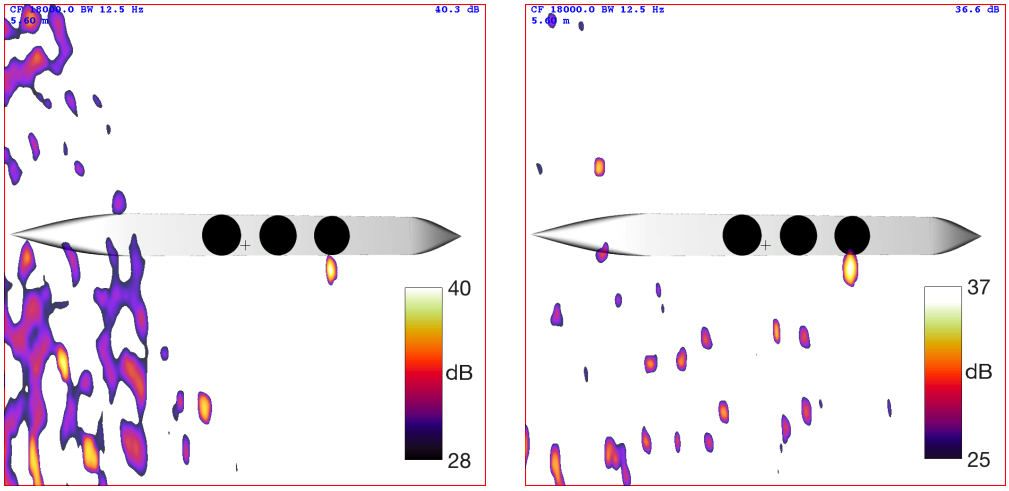

(a) No DR, no subtraction **(b) No DR, subspace subtraction**

Figure 9. Comparison of DAMAS2 18 kHz narrowband deconvolution results for 40- by 80-Foot Wind Tunnel data. All images have a 12-dB dynamic range.

when the leading edge is drooped. This situation corresponds to simulated Cases 3 and 5, where conventional subtraction can yield underpredicted levels, but subspace subtraction appears reliable. Below 6 kHz the wing tip sources appear to increase in magnitude when the leading edge is drooped. This situation corresponds to simulated Cases 2 and 4, where both subtraction methods do not remove enough of the background signal. The behavior is in agreement with the suspicion from the isolated spectral analysis of these data in the previous section, which suggested a significant amount of the background signal remains post-subtraction. Investigation of the irregular diagonal removal behavior for the background data below 4 kHz is warranted, but beyond the scope of this study.

The oblique subtraction analysis procedure allows the calculation of the angle between the signal and background subspace estimates in the data. The computed results indicate that the orthogonality assumption is invalid for some frequencies, and are shown in Fig. 12. The method predicts orthogonal (90 degree) subspaces for lower frequencies, but just below 10 kHz begins to predict a more acute angle, approaching 60 degrees by 20 kHz. This prediction, in conjunction with the similarity of the majority of the high frequency results between methods, suggests that the subspace orthogonality requirement is not strict when considering integrated levels from deconvolution methods.

As with the inflow data, two segments of the plotted bandwidth show noticeable disagreement between the spectra. A strong spike is noticeable just below 17 kHz. This spike is due to a contaminating signal, likely electrical, which is present in the acquisition and coherent between a small subset of the array microphones. The levels and channel-to-channel coherence of this spike change between the source and background acquisitions, violating the requirements of these subtraction methods. Narrowband deconvolution maps at these discrete frequencies, for the most part, are sufficiently contaminated such that no actual acoustic sources are discernible. Oblique subtraction is the one exception, where depending on plot parameters the deconvolution maps can show the expected aeroacoustic noise sources along with some remaining contamination. Due to the difficulty of visual interpretation, the narrowband plots of these frequencies are omitted from this work. However, the overall influence on the narrowband data summed into the 16 kHz one-third octave band is shown in Fig. 13, where the orthogonal and oblique subspace subtraction data are contrasted. For display purposes, images are interpolated to a resolution four times that used in the deconvolution process. The significant spreading of the side edge acoustic sources is attributed to decorrelation effects.[22] It is immediately evident that oblique subtraction provides better rejection of the signal contamination. The superior filtering provided by the oblique subtraction method is currently not fully understood, as the contamination

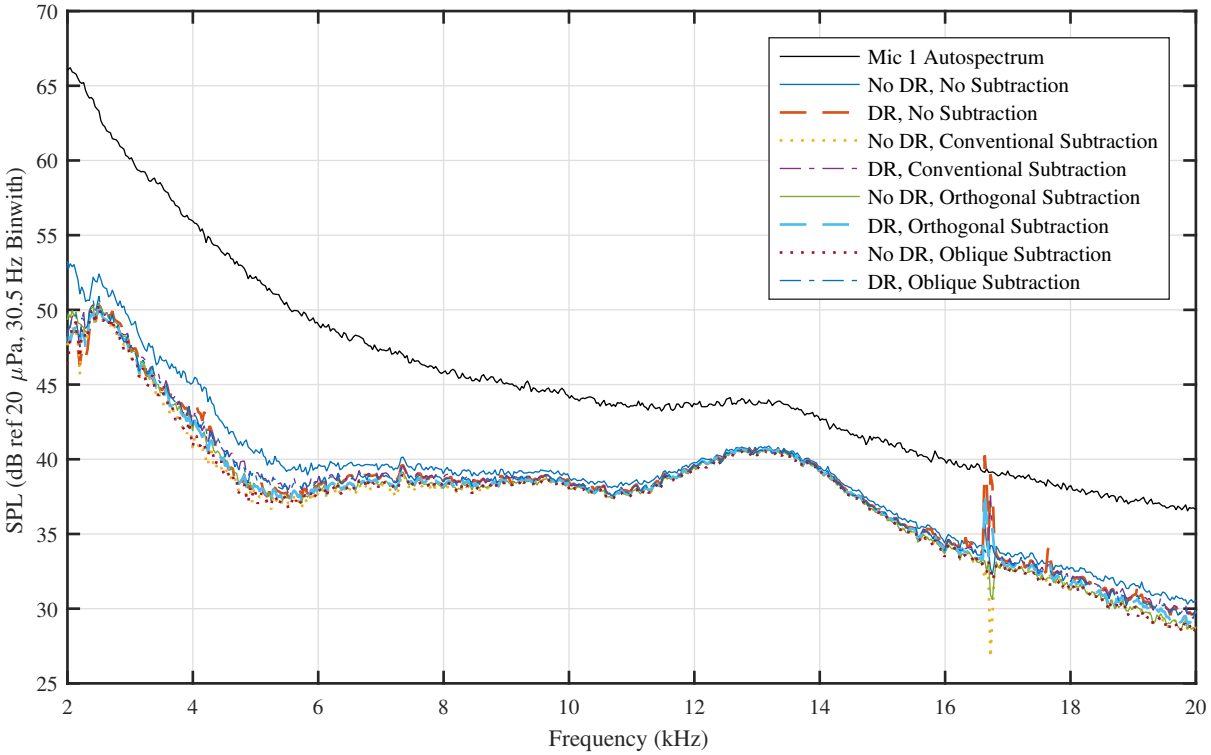

Figure 10. Comparison of DAMAS drooped leading edge side edge integrated spectra results for 14- by 22-Foot Wind Tunnel data.

changed significantly between acquisitions. However, it is suspected that this is due to the oblique subtraction process incorporating a physical model of the signal subspace in addition to using a data-driven model of the background subspace.

The second band considered is for frequencies below approximately 7 kHz. Here, the baseline (no diagonal removal, no background subtraction) integrated level diverges from the rest of the data, and the remaining methods show some more variability in their output. As an example of this band, the 4 kHz results are plotted in Fig. 14. For ease of interpretation, one-third octave bands are again used. The baseline data without diagonal removal are plotted in Fig. 14a as it shows significant difference in integrated levels. The orthogonal subtraction results without diagonal removal are shown in Fig. 14b as characteristic of all the other curves, which have similar integration levels and similar deconvolution maps. Subtraction significantly reduces the extent of the wing tip vortices even if it cannot remove them. The drooped leading edge side edges show a minor reduction in extent, though not as dramatic as the wing tip vortices.

8. Summary & Conclusions

A subspace-based form of background subtraction is presented and applied to aeroacoustic wind tunnel data. The background subtraction method identifies eigenvalue-eigenvector combinations in a CSM, which are related to background noise sources, and removes them under the assumption that background noise eigenvectors are orthogonal to signal-of-interest eigenvectors.

The subspace-based subtraction technique shows improved, more robust behavior when compared to conventional background subtraction using simulated data. While the technique may still fail under a variety of conditions, it does not appear to fail in a situation where conventional subtraction succeeds. It does succeed in situations where conventional subtraction fails. The technique also provides the benefit

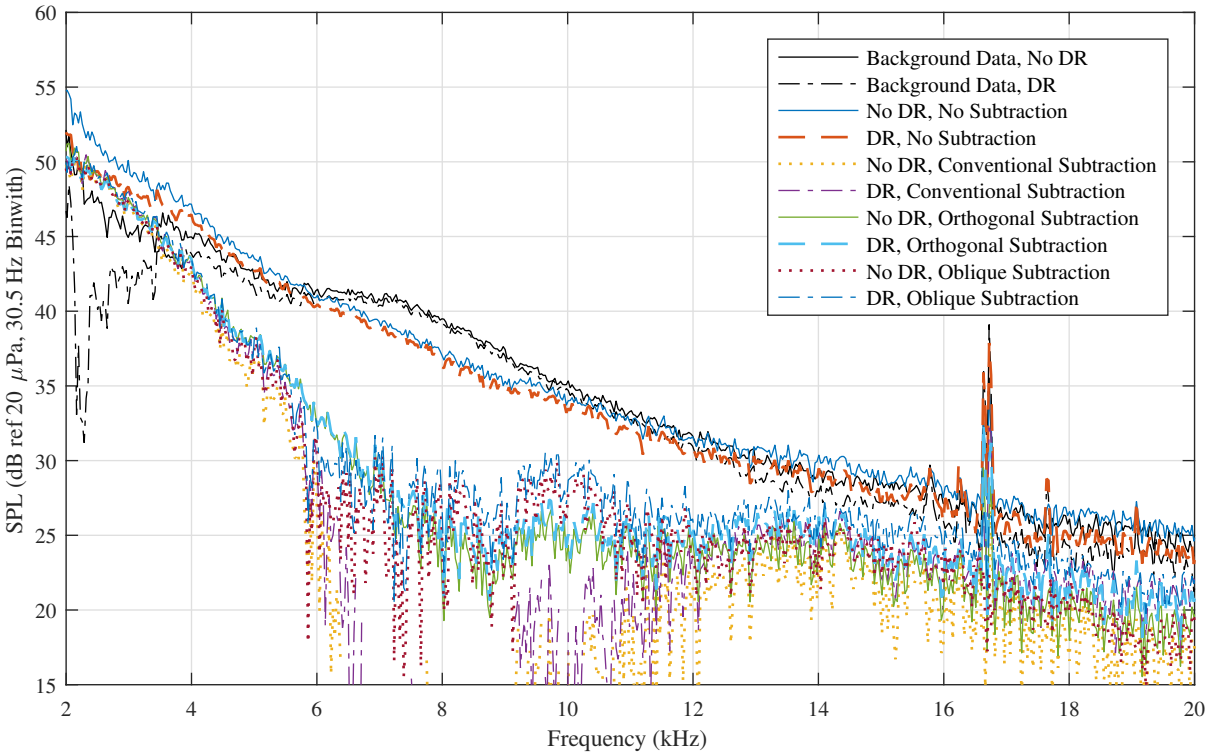

Figure 11. Comparison of DAMAS wing tip integrated spectra results for 14- by 22-Foot Wind Tunnel data. Note that ideally any subtraction method would yield a wing tip spectrum with zero power.

of maintaining a positive semidefinite CSM, and thus computing physical coherence relationships between channels in the CSM.

Application to auto- and cross-spectra from tests in both closed-wall and open-jet wind tunnels shows significant differences between subtraction techniques in poor signal-to-noise ratio conditions. The subspace-based subtraction technique shows some ability to reconstruct an expected spectral shape for data where conventional subtraction cannot. While the new method still appears to fail for sufficiently weak signal data, it maintains usable signal-to-noise and coherence estimates that allow for assessment of data quality. Both conventional and subspace-based subtraction allow for some separation of two distinct aeroacoustic noise sources, although the subspace-based subtraction provides more consistent behavior at frequencies where conventional subtraction fails. A more expensive oblique subtraction method is the only technique that can mitigate strongly-correlated contamination, when the contamination changes significantly between background and source acquisitions. The oblique method shows that, aside from such contamination, the orthogonality requirement for subspace subtraction is not strict. This is observed in the behavior of the orthogonal subtraction technique when oblique subtraction gives an acute angle of 60 degrees between subspaces.

Deconvolution results show that for the most part integrated levels are insensitive to parameter selection in terms of diagonal removal and background subtraction method. If no background subtraction is applied and correlated acoustic contamination is present, diagonal removal may prove insufficient in mitigating the contamination. This depends both on the integration bound selection and on whether the deconvolution map bounds capture the contaminating noise sources. When signal-to-noise becomes sufficiently poor and/or the data model begins to break down, no method appears to provide reasonable estimates of source level and behavior.

In summary, the proposed background subtraction method allows an alternative background subtraction

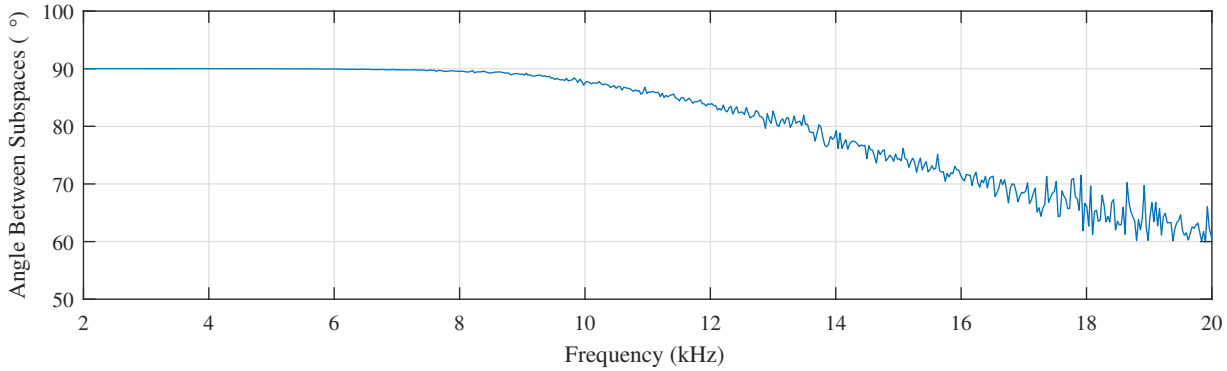

Figure 12. Estimated angle between signal and background subspaces for the 14- by 22-Foot Wind Tunnel data.

calculation that, while still limited, is more robust to fluctuations in background noise between background and source acquisitions when compared to conventional subtraction. The method provides a means to maintain the positive semidefinite property of the predicted CSMs, giving an advantage over conventional subtraction. For the considered data, it provides superior results in estimates of auto- and cross-spectra, and allows the estimation of signal-to-noise ratios and coherence. However, it shows little improvement over conventional subtraction in terms of integrated deconvolution levels. The minimal increase in computational expense of the technique when compared to conventional subtraction suggests it can be used as a general replacement for conventional subtraction. When subtraction is used with an appropriate background CSM, diagonal removal appears unnecessary. The more expensive oblique subtraction technique can partially succeed in circumstances where both conventional and orthogonal subtraction fail, and should be further investigated for cases of data contamination which varies significantly between tests.

Acknowledgments

This work was funded by the NASA Environmentally Responsible Aviation and Advanced Air Transport Technology Projects. The authors also wish to acknowledge the efforts of research and test staff at both NASA Langley and NASA Ames for their dedicated work with the N2A-EXTE and AMELIA CESTOL tests. In particular, they thank Nathan Burnside from NASA Ames for his efforts in processing the microphone phased array results from the 40- by 80-Foot Wind Tunnel test.

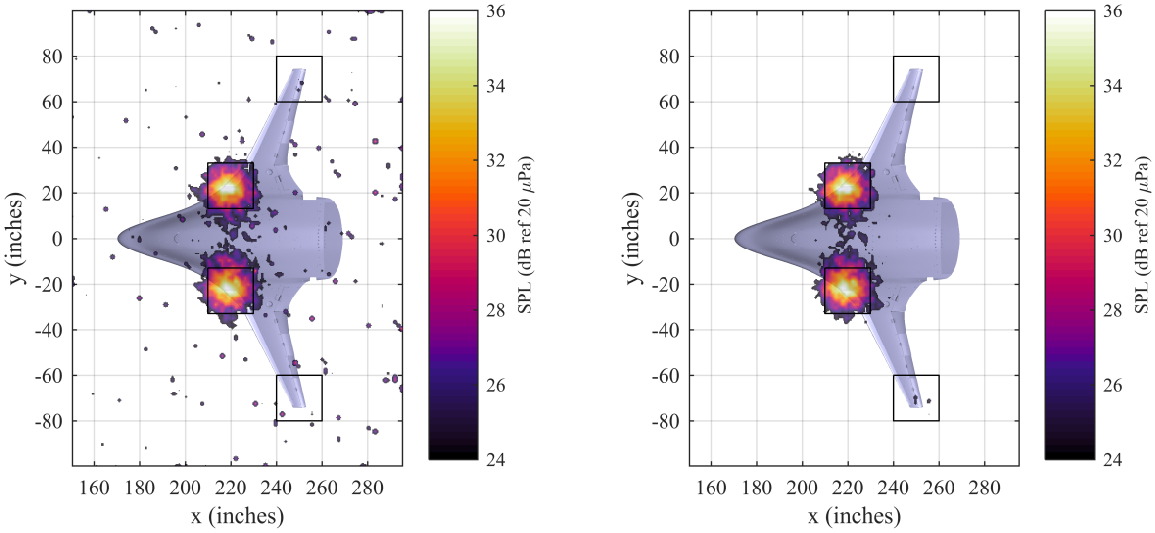

(a) No DR, orthogonal subtraction **(b) No DR, oblique subtraction**

Figure 13. Comparison of DAMAS 16 kHz 1/3rd-octave band deconvolution results for 14- by 22-Foot Wind Tunnel data, showing the influence of subspace assumptions. Integration bounds for the narrowband results are shown as black boxes around the leading edge side edges and wing tips.

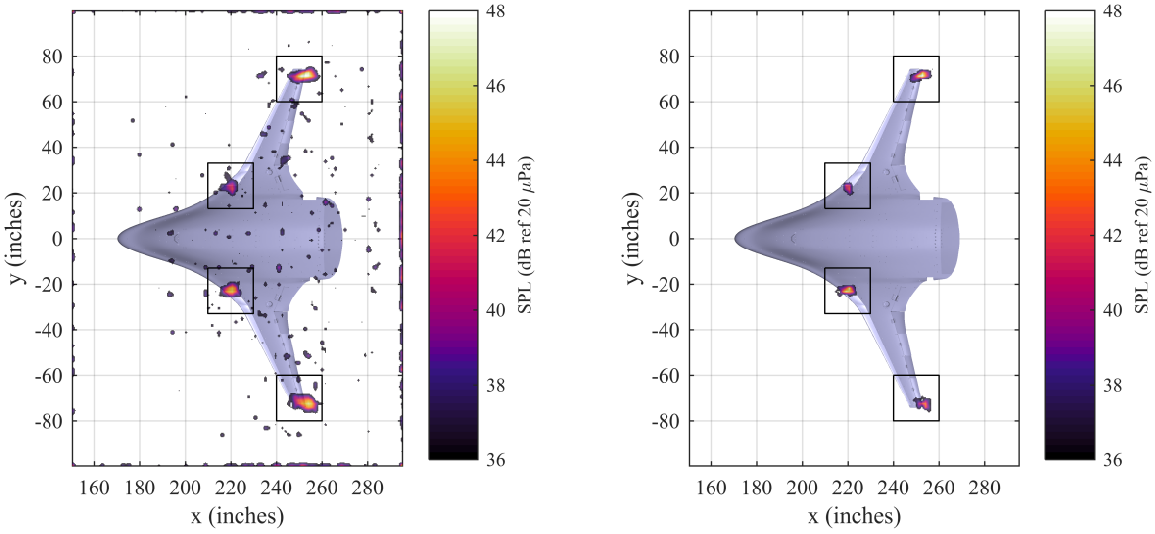

(a) No DR, no subtraction **(b) No DR, orthogonal subtraction**

Figure 14. Comparison of DAMAS 4 kHz 1/3rd-octave band deconvolution results for 14- by 22-Foot Wind Tunnel data. Integration bounds for the narrowband results are shown as black boxes around the leading edge side edges and wing tips.

References

[1] Dougherty, R. P., *Aeroacoustic Measurements,* T. J. Mueller, Ed., chap. 2. Beamforming in Acoustic Testing, Springer-Verlag, Berlin, Heidelberg & New York, 2002, pp. 62–97.

[2] Bahr, C. J., Brooks, T. F., Humphreys, W. M., Spalt, T. B., and Stead, D. J., "Acoustic Data Processing and Transient Signal Analysis for the Hybrid Wing Body 14- by 22-Foot Subsonic Wind Tunnel Test," AIAA 2014-2345, 20$^{\text{th}}$ AIAA/CEAS Aeroacoustics Conference, AIAA Aviation 2014, Atlanta, GA, June 2014.

[3] Humphreys, W. M., Brooks, T. F., Hunter, W. W., and Meadows, K. R., "Design and Use of Microphone Directional Arrays for Aeroacoustic Measurements," AIAA-98-0471, 36$^{\text{th}}$ AIAA Aerospace Sciences Meeting & Exhibit, Reno, NV, January 1998.

[4] Horne, W. C., "Initial Assessment of Acoustic Source Visibility with a 24-element Microphone Array in the Arnold Engineering Development Center 80- by 120-Foot Wind Tunnel at NASA Ames Research Center," AIAA 2011-2723, 17$^{\text{th}}$ AIAA/CEAS Aeroacoustics Conference, Portland, OR, June 2011.

[5] Bahr, C. J., Yardibi, T., Liu, F., and Cattafesta, L. N., "An Analysis of Different Measurement Techniques for Airfoil Trailing Edge Noise," AIAA 2008-2957, 14$^{\text{th}}$ AIAA/CEAS Aeroacoustics Conference, Vancouver, BC, May 2008.

[6] Spalt, T. B., Fuller, C. R., Brooks, T. F., and Humphreys, W. M., "A Background Noise Reduction Technique using Adaptive Noise Cancellation for Microphone Arrays," AIAA 2011-2715, 17$^{\text{th}}$ AIAA/CEAS Aeroacoustics Conference, Portland, OR, June 2011.

[7] Blacodon, D., "Array Processing for Noisy Data: Application for Open and Closed Wind Tunnels," *AIAA Journal*, Vol. 49, No. 1, January 2011, pp. 55–66.

[8] Dougherty, R. P., "Source Location with Sparse Acoustic Arrays; Interference Cancellation," DNW, 1$^{\text{st}}$ CEAS-ASC Workshop: Wind Tunnel Testing in Aeroacoustics, 5-6 November, 1997.

[9] Oerlemans, S. and Sijtsma, P., "Determination of absolute levels from phased array measurements using spatial source coherence," NLR-TP-2002-226, NLR, 2002.

[10] Sarradj, E., "A fast signal subspace approach for the determination of absolute levels from phased microphone array measurements," *Journal of Sound and Vibration*, Vol. 329, No. 9, 2010, pp. 1553–1569.

[11] Suzuki, T., "L_1 generalized inverse beam-forming algorithm resolving coherent/incoherent, distributed and multipole sources," *Journal of Sound and Vibration*, Vol. 330, No. 24, 2011, pp. 5835–5851.

[12] Bulté, J., "Acoustic Array Measurements in Aerodynamic Wind Tunnels: a Subspace Approach for Noise Suppression," AIAA 2007-3446, 13$^{\text{th}}$ AIAA/CEAS Aeroacoustics Conference, Rome, Italy, 2007.

[13] Allen, M. R. and Smith, L. A., "Optimal filtering in singular spectrum analysis," *Physics Letters A*, Vol. 234, October 1997, pp. 419–428.

[14] Sekihara, K., Hild, K. E., Dalal, S. S., and Nagarajan, S. S., "Performance of Prewhitening Beamforming in MEG Dual Experimental Conditions," *IEEE Transactions on Biomedical Engineering*, Vol. 55, No. 3, March 2008, pp. 1112–1121.

[15] Moler, C., *Numerical Computing with MATLAB*, chap. 10. Eigenvalues and Singular Values, The MathWorks, 2013, pp. 1–39.

[16] Higham, N. J., "Computing a Nearest Symmetric Positive Semidefinite Matrix," *Linear Algebra and its Applications*, Vol. 103, 1988, pp. 103–118.

[17] D'Errico, J., "nearestSPD (http://www.mathworks.com/matlabcentral/fileexchange/42885-nearestspd)," (last accessed March 24, 2015), 2013.

[18] Heath, S. L., Brooks, T. F., Hutcheson, F. V., Doty, M. J., Bahr, C. J., Hoad, D., Becker, L. E., Humphreys, W. M., Burley, C. L., Stead, D. J., Pope, D. S., Spalt, T. B., Kuchta, D. H., Plassman, G. E., and Moen, J. A., "NASA Hybrid Wing Body Aircraft Aeroacoustic Test Documentation Report," Tech. Rep. NASA TM-2016-219185, April 2016.

[19] Humphreys, W. M., Brooks, T. F., Bahr, C. J., Spalt, T. B., Bartram, S. M., Culliton, W. G., and Becker, L. E., "Development of a Microphone Phased Array Capability for the Langley 14- by 22-Foot Subsonic Tunnel," AIAA 2014-2343, 20$^{\text{th}}$ AIAA/CEAS Aeroacoustics Conference, AIAA Aviation 2014, Atlanta, GA, June 2014.

[20] Horne, W. C. and Burnside, N. J., "AMELIA CESTOL Test: Acoustic Characteristics of Circulation Control Wing and Leading- and Trailing-Edge Slot Blowing," AIAA 2013-0978, 51$^{\text{st}}$ AIAA Aerospace Sciences Meeting, Dallas/Ft. Worth, TX, January 2013.

[21] Horne, W. C. and Burnside, N. J., "Development of New Wall-mounted and Strut-mounted Phased Microphone Arrays for Acoustic Measurements in Closed Test-section Wind Tunnels," AIAA 2015-2975, 21$^{\text{st}}$ AIAA/CEAS Aeroacoustics Conference, Dallas/Ft. Worth, TX, June 2015.

[22] Hutcheson, F. V., Spalt, T. B., Brooks, T. F., and Plassman, G. E., "Airframe Noise from a Hybrid Wing Body Aircraft Configuration," AIAA 2016-2708, 22$^{\text{nd}}$ AIAA/CEAS Aeroacoustics Conference, Lyon, France, May 2016.

[23] Dougherty, R. P., "Extensions of DAMAS and Benefits and Limitations of Deconvolution in Beamforming," AIAA-2005-2961, 11$^{\text{th}}$ AIAA/CEAS Aeroacoustics Conference, Monterey, CA, May 2005.

[24] Dougherty, R. P., "Turbulent Decorrelation of Aeroacoustic Phased Arrays: Lessons from Atmospheric Science and Astronomy," AIAA-2003-3200, 9$^{\text{th}}$ AIAA/CEAS Aeroacoustics Conference, Hilton Head, SC, May 2003.

[25] Brooks, T. F. and Humphreys, W. M., "A deconvolution approach for the mapping of acoustic sources (DAMAS) determined from phased microphone arrays," *Journal of Sound and Vibration*, Vol. 294, 2006, pp. 856–879.

[26] Bahr, C. J. and Horne, W. C., "Advanced Background Subtraction Applied to Aeroacoustic Wind Tunnel Testing," AIAA 2015-3272, 21$^{\text{st}}$ AIAA/CEAS Aeroacoustics Conference, AIAA Aviation 2015, Dallas/Ft. Worth, TX, June 2015.

[27] Yardibi, T., Li, J., Stoica, P., Zawodny, N. S., and Cattafesta, L. N., "A covariance-fitting approach for correlated acoustic source mapping," *Journal of the Acoustical Society of America*, Vol. 127, No. 5, May 2010, pp. 2920–2931.